Optical and Quantum Electronics (2022) 54:590
https://doi.org/10.1007/s11082-022-04003-0

Hybrid polymer–glass planar Bragg grating as a temperature and humidity sensor

D. Mares[1] · V. Prajzler[1] · T. Martan[1] · V. Jerabek[1]

Received: 26 December 2021 / Accepted: 13 July 2022 / Published online: 3 August 2022

Abstract
This paper presents the design and construction of a new planar optical Polymer Waveguide Bragg grating (PWBG) temperature and humidity sensor realized by polymer-glass hybrid technology composition with a new layout concept. The Bragg grating of a sensor was made by a Direct Laser Writing (DLW) in Poly (methyl methacrylate) (PMMA) formed on a multimode waveguide realized in a glass substrate by $Ag^{+} \leftrightarrow Na^{+}$ ion exchange. The fabricated hybrid Bragg grating structure exhibited more than 10 dB of the attenuation dip, equivalent to higher than 90% diffraction efficiency. The fabricated hybrid PWBG sensor exhibited high temperature and humidity sensitivity in contrast to glass-based sensors of − 48.6 pm/°C and 54.16 pm·RH^{-1}, respectively.

Keywords Polymer Bragg grating sensor · Multimode glass waveguide · PMMA · Laser-thermal patterning

1 Introduction

Over the last few decades, the planar optical Polymer Waveguide Bragg Grating (PWBG) sensors and the Polymer Fiber Bragg Grating (PFBG) sensors have been subjects of intense research and applications. The very good properties of some transparent polymers are the high temperature and humidity coefficients, which allow PWBG sensor implementation. Because of the broad diversity of optical polymers and their properties, optimization of the structural characteristics for the selected application area can be easily achieved. Furthermore, it is well suited for the increasingly demanding requirements for optical sensor performance, degree of integration, and the cost-effectiveness of modern optical PWBG sensors. The use of traditional acrylates or epoxy polymer sensors results in typical temperature sensitivity of more than − 40 pm/°C (Caroll et al. 2007; Liu et al. 2001; Beneitez et al. 2005; Zhang and Tao 2013), relative humidity (RH) of 42 pm/RH or strain 2.04 pm/με (Rosenberg et al. 2012, 2014). In the past, many methods of implementing PWBG have been proposed for different types of polymers. The most common lithographic method is

✉ V. Jerabek
jerabek@fel.cvut.cz

[1] Department of Microelectronics, Faculty of Electrical Engineering, Czech Technical University in Prague, Technická 2, Prague 16627, Czech Republic

contact UV photolithography, where the diffraction limit determines the constant periodicity of the grating in units of micrometers. Using new technologies such as EBL ion beam recording (Aubry et al. 2002), advanced X-ray photolithographic techniques (Reznikova et al. 2008), EBL electron beam lithography (Wong et al. 2003), or nanoimprinting (Binfeng et al. 2014), it is possible to produce a grid with a fine grid period in the hundreds of nanometers. The fiber Bragg gratings (FBGs) in polymer optical fibers (POFs) based on Poly (methyl methacrylate) (PMMA) have been reported in both step-index of refraction by Yu et al. (2004), and microstructure fibers by Dobb et al. (2005). The temperature sensitivity of polymer FBGs is more than that ten times higher than silica fiber gratings. Sherman and Zappe (2014) presented planar PWBG fabricated by replication technology. He proved that PMMA is the most suitable material for temperature sensors if we compare the value of thermal expansion and thermo-optical coefficient of different polymers. The value of the thermo-optic coefficient of PMMA is set by Polystyrene (PS) mixing. The refractive indices for the PS and PMMA copolymers show a linear relationship to styrene volume at room temperature as presented in Johnson and Town (2015). The refractive indices for the PS and PMMA copolymers show a linear relationship with styrene volume at room temperature of 1.49–1.57. This increase can be used to modify the Bragg wavelength. PWBGs realized by replication technology by using RIE with a very low grating period of 200 nm are published in a paper by Sherman and Zappe (2014). In this work, it is demonstrated that, under a particular condition, the relation of the Bragg wavelength dependence on temperature could be progressive and nonlinear depending on the crosslinking, chain length, and molecular weight of the monomer. In the majority of reported applications Bragg Grating (BG) works in a single-mode regime. However, BG was used in few-mode, and the multimode regime, delivering a wider wavelength band, was also presented by Mizunami et al. (2000). A hybrid temperature sensor realized by deposited polymer layers on a curved side-polished single-mode fiber with polymer Bragg grating is presented in the paper presented by Ouerghia et al. (2005). The cladding is locally removed to gain access to the evanescent field of the guided mode. The structure is then coated by the polymer. The deposited polymers are susceptible to a temperature change through the thermo-optic effects.

The purpose of this paper is to report on the design, fabrication, and utilization of a new layout concept PWBG temperature and humidity sensor created by a planar polymer-glass hybrid composition. Our concept uses a combination of the ion-exchanged glass waveguide and a PMMA polymer BG. For the creation of polymer BG, a Direct Laser Writing method (DLW) using the Marangoni phenomenon was used. The application of this method has been published previously in Mares and Jerabek (2016) based on the principal work of Lyutakov et al. (2009). The theoretical modeling of the radiation field profile of the cladding thickness and dimensions of the grating was created by the mathematical solution and optimization of the wave equation using Beam Propagation Method (BMP) and Rigorous RCWA methods utilizing simulation software. The temperature and humidity coefficients of the implemented sensor were measured and compared with the calculated ones.

2 Design of the hybrid PWBG sensor

The design was done using the planar hybrid technology combining two technological and material approaches. These two technology steps include the fabrication of optical channel waveguides by an ion exchange process in the glass substrate and the fabrication polymer layer with Bragg grating (BG) onto channel waveguides. This concept leads to the

interconnection of the optical light propagated in the channel waveguide core and controlled by the light connected via the polymer layer with the BG structure by an evanescent wave. The proposed sensor structure is presented in Fig. 1. Figure 1a shows the three-dimensional model and Fig. 1b shows the front view and the cross-sectional view of the hybrid PWBG. The BG is realized as a surface corrugation of the upper side of the surface PMMA layer. An optical diffused channel waveguide with a diameter of 4 μm was fabricated by $Ag^+ \leftrightarrow Na^+$ ion exchange into sodium glass substrate (Barkman et al. 2013). The waveguide had a refractive index of the glass substrate $n_s = 1.492$, and the refractive index difference of the channel core waveguide was $\Delta n = 0.003$ for wavelength of 1310 nm.

One-step ion exchange $Ag^+ \leftrightarrow Na^+$ into the glass substrate was applied to achieve a high coupling coefficient between the channel waveguide and BG structure fabricated in the PMMA layer. The BG grating was fabricated by the DLW method into a thin PMMA layer doped with the dye additive Porphyrine to a sensitive DLW optical source of 405 nm. The refractive index of the doped PMMA was set to be $n_c = 1.485$ slightly lower than the index of refraction of the channel core waveguide.

2.1 The PWBG sensor parameters

The crucial first parameter of the sensor is the central operational Bragg wavelength λ_B, which can be obtained from the condition for wave phase synchronization between the glass ion exchange waveguide and the BG created in the polymer cladding (1). The effective refractive index n_{eff} was determined by BPM simulations for the Bragg wavelength.

$$\Lambda = \frac{\lambda_{\mathrm{B}}}{2n_{\mathrm{eff}}}|q|, \quad q = 0, \pm 1, \pm 2 \tag{1}$$

where q is the grating diffraction order, which in our design was $q = 3$. The grating period and the order of the diffraction were set because of the limitation of the used DLW

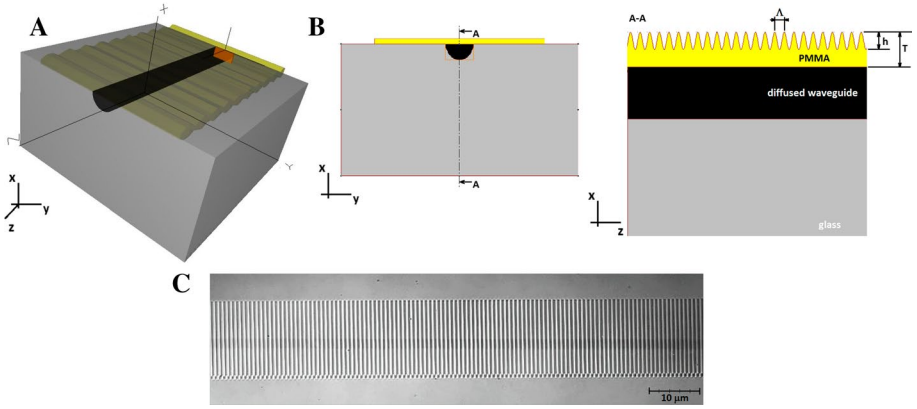

Fig. 1 **a** Three-dimensional model of the sensor structure consisting of the glass substrate, ion exchange waveguide channel, and topside corrugated cladding PMMA BG layer; **b** Front view and cross-section (A–A) view of the hybrid PWBG and cross-section (A–A) view of the hybrid PWBG. Λ is the period of the grating, h is the depth of the groove, and T is the thickness of the polymer layer; **c** Topside image of the fabricated structure where the longitudinal darker line is the ion channel waveguide, and the perpendicular lines are forming the grating

technique exploiting the Marangoni effect. The lower grating orders exhibited either defects, non-periodic patterns, or insufficient modulation ratio of the grating. The calculated grating periods of PWBG for the first three orders Λ_q are summarized in Table 1.

The next parameter that must be considered is the thickness of the polymer layer T. To determine the optimum thickness of the polymer layer, the electric field strength E_y in the x-direction was solved using a 2D wave equation.

Using wave Eq. (2) for the radiation propagating in the waveguide with the gradual changes of the refractive index, we derive the electrical distribution field profile equation E_y for waveguide core diffused layer (3) and a grating cladding layer (4) in the x-axis, see Fig. 3,

$$\frac{d^2E_{\mathrm{y}}}{dx^2} + (k^2(x) - \beta^2)E_y = 0 \tag{2}$$

$$\frac{d^2E_{\mathrm{yf}}}{dx^2} + (k_0^2(n_s^2 + \delta e(-x/d)) - \beta^2)E_{yf} = 0 \tag{3}$$

$$\frac{d^2E_{yc}}{dx^2} + (k_0^2n_c^2 - \beta^2)E_{yc} = 0 \tag{4}$$

where k is the wave number, k_0 is the free space wave number, β is the propagation constant along the direction of the z-axis, n_s is the substrate refractive index, n_c is the refractive index of the PMMA cladding, d is the depth of diffusion, and is approximated by $\delta = 2n_s\Delta n$.

The calculation performed using Eqs. (3) and (4) reveals in Fig. 2 that the maximal reasonable value of the thickness cladding layer is $T = 2$ µm. The thicker layer does not further enhance the transfer of energy from the guided wave to the evanescent wave of the polymer layer with BG. This boundary condition was considered in the following optimization through simulations.

RSoft BeamPROP and GratingMOD software packages were used for the design and optimization of the waveguide structure, the mode coupling, and the BG structure, respectively. The simulations focused on optimizing the thickness of the polymer grating layer T, the grating period for third-order diffraction $\Lambda_{q\text{-}3}$, the grating length L, and grating modulation ratio h/T (modulation depth/thickness of the layer) to maximize the diffraction efficiency η. From the calculation and a common-sense point of view, the best interaction with the grating is expected to be in the close vicinity of the waveguide. However, taking to account the limitation of the DLW fabrication technology used, the achievable modulation depth of the cladding layer is depicted in Table 2.

The optimal thickness of the grating layer was found to be $T_{opt} = 500$ nm for the coupling coefficient $\kappa = 4.53$ cm^{-1}, resulting in the diffraction efficiency $\eta = 0.18$ for the length of the grating $L = 1$ mm. The diffraction efficiency is directly proportional to the grating

Table 1 Calculated grating periods $\Lambda_{q\text{-}1}$, $\Lambda_{q\text{-}2}$, and $\Lambda_{q\text{-}3}$ of PWBG for different grating orders and Bragg wavelength λ_B

λ_B (nm)	n_{eff} (–)	$\Lambda_{q\text{-}1}$ (nm)	$\Lambda_{q\text{-}2}$ (nm)	$\Lambda_{q\text{-}3}$ (nm)
1175	1.4884	395	790	1185

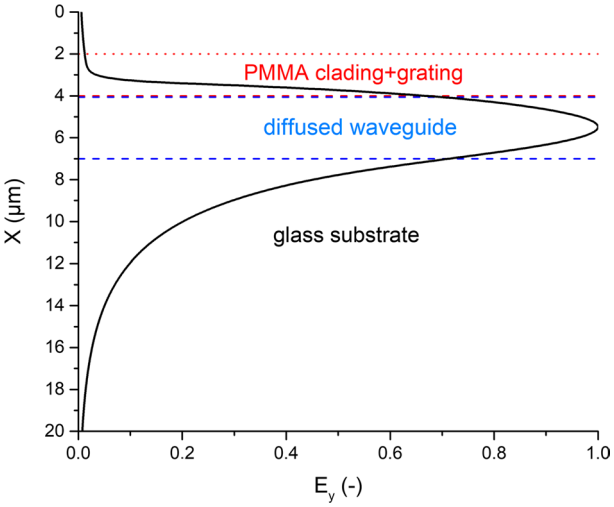

Fig. 2 The arb. unit field profile E_y in the cross-section (A–A) view of the hybrid PWBG

Table 2 The calculated diffraction efficiency for the different thicknesses T, the depth of the groove h for the length of the grating with $L = 1000$ μm

T (nm)	h (nm)	η (–)
730	270	0.144
500	180	0.18
400	130	0.15
220	30	0.015

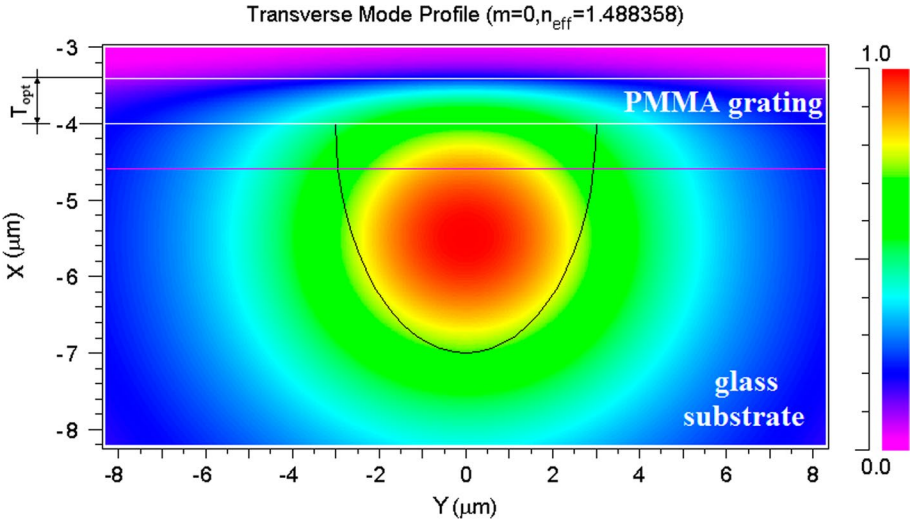

Fig. 3 Electrical field distribution profile of the transversal mode TE_0 in the core of the optical diffused channel waveguide for the PWBG structure. BG is located in the PMMA cladding layer

length. Therefore, the necessary increase in the length of the grating to $L=5$ mm in the hybrid structure was calculated to obtain a diffraction efficiency $\eta > 95\%$.

Simulation of the electrical fundamental transversal mode TE_0 distribution indicates that an evanescent part of the guided light in the core penetrates the cladding layer and interacts with the grating. The refraction indices, the optimal thickness of the cladding layer, and the degree of the core submersion had been optimized to allow maximum interaction between the cladding layer and the submersed core waveguide without leakage of the guided mode from the diffused waveguide. The field distribution profile simulation of the electrical transversal mode TE_0 in the optical diffused channel waveguide for the PWBG structure is shown in Fig. 3.

Thermally-induced changes of the index n_{eff} and the grating period Λ in the PWBG induce a shift in the Bragg wavelength of the grating $\Delta\lambda_B$. For a PWBG with small uniform temperature changes ΔT, these individual effects can be superimposed to produce the Bragg wavelength shift (5),

$$\frac{\Delta\lambda_B}{\lambda_B} = \frac{\Delta n_{eff}}{n_{eff}} + \frac{\Delta\Lambda}{\Lambda} \tag{5}$$

where dn_{eff}/n_{eff} represents the change in the index of refraction and $\Delta\Lambda/\Lambda$ is the contribution of thermal expansion resulting from a change in temperature ΔT.

The change in the effective index of refraction n_{eff} can be expressed by the thermo-optical coefficient dn_{eff}/dT of the material and α' coefficient of thermal expansion with the temperature change ΔT as

$$\frac{\Delta\lambda_B}{\lambda_B} = \frac{dn_{eff}}{dT}\Delta T + \alpha'\Delta T \tag{6}$$

Typical values for dn_{eff}/dT for glassy polymers range of $-1\cdot10^{-4}$ to $-2\cdot10^{-4}$ °C^{-1} (Weber 1995); the relative change of the grating period due to thermal expansion is given by

$$\frac{\Delta\Lambda}{\Lambda} = \alpha'\Delta T \tag{7}$$

where α' is the linear coefficient of thermal expansion.

Since the change in the grating period is affected only by the expansion change in one dimension along the grating, the linear coefficient of thermal expansion α' has to be used. The typical PMMA values of the linear thermal expansion coefficient are $(15–30)\cdot10^{-6}$ °C^{-1} (Weber 1995).

Thus, the two contributions to the wavelength shift due to thermo-optical and thermal expansion effects are opposite in signs. Therefore, the Bragg wavelength change $\Delta\lambda_B$ can be shifted to lower or higher wavelengths, depending on the polymer used and its properties. The polymer PMMA forming the grating layer was obtained from Good Fellow Inc. and the catalog values of dn/dT and α' are $-1.1\cdot10^{-4}$ °C^{-1} and $26\cdot10^{-6}$ °C^{-1}, respectively. Substituting these values into (6), the shift of the λ to the lower wavelengths with temperature is expected. The calculated value is -56.6 pm/°C.

The effect of changes in humidity on the PWBG affects the grating constant to a similar extent as in the case of temperature changes. The absorption of water molecules changes the effective refractive index of the polymer layer and is simultaneously accompanied by an increase in the volume of the structure and subsequently the grating period, resulting in a change in the Bragg wavelength. The dry and wet PMMA refractive index values for the

change in humidity used in the theoretical model were experimentally obtained by Rosenberger et al. (2014). The relative refraction change of the effective relative index of refraction was set at $dn_{eff}/dRH = 8.053 \cdot 10^{-6}$. The extension of the grating period $\Delta\Lambda/\Lambda$ due to changes in humidity changes $\zeta = 2.123 \cdot 10^{-5}$.

The variation of the Bragg wavelength with humidity can be expressed by Eq. (8) and by fitting the values for PMMA to the form (9):

$$\frac{\Delta\lambda_B}{\lambda_{B1}} = \frac{dn_{eff}}{dRH}\Delta RH + \zeta\Delta RH \tag{8}$$

$$\frac{\Delta\lambda_B}{\lambda_{B1}} = \left(8053 \cdot 10^{-6} + 2123 \cdot 10^{-5}\right)\Delta RH \tag{9}$$

where ΔRH is the change in relative humidity (0–100%), ζ is the parameter of the length extension of PMMA grating due to the absorption of water molecules.

2.2 Fabrication

The fabrication process is shown in Fig. 4 step by step. In the first step, the glass wafer was cut and polished (Fig. 4a). Then photolithography process (Fig. 4b) was used for defining the diffusion region by a slit of width w in the lithographic mask deposited on the substrate surface. The deposition of the lithographic mask is done by etching. A thin layer of titanium with a thickness of approximately 150 nm was deposited on the surface free of impurities followed by the deposition of the positive photoresist AZ1518S by spin-coating. After alignment of the lithographic mask and exposure of the wafer surface to a UV source on a JUB 2104 lithography machine, the substrate wafer was passed through an AZ-D300S developer to remove the exposed area of the photoresist. The photoresist remaining on the wafer surface defined the

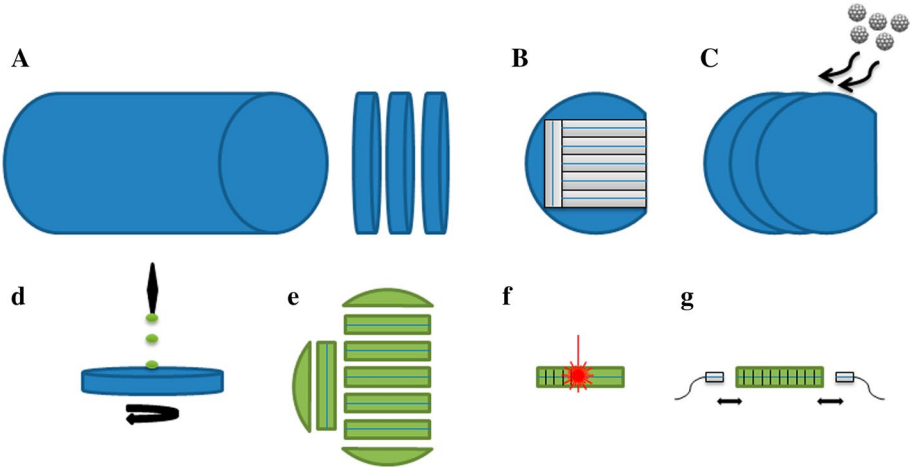

Fig. 4 The hybrid PWBG sensor fabrication procedure: **a** wafer cutting and polishing, **b** photolithography, **c** ion exchange, **d** polymer spin coating, **e** chip cutting and polishing, **f** grating formation, **g** fiber-chip coupling (Mares and Jerabek 2016)

titanium layer area, which was etched in NaOH solution. In the last stage of the lithographic mask deposition process, the photoresist layer was removed in AZ-Rem1165 solvent and after cleaning, the wafer was subjected to optical inspection on an electron microscope to verify the quality of the preparation for subsequent fabrication of the channel waveguides by one-step ion exchange $Ag^+ \leftrightarrow Na^+$ (Fig. 4c).

Prepared glass substrate containing Na^+ ions is placed in a melt containing chemically similar elements, in this case, Ag^+. At the interface between the substrate and the melt, the concentrations of the two types of ions involved in the ion exchange decrease dramatically. This fact leads to a non-equilibrium state and the formation of a concentration gradient. Due to the high temperature, random collisions occur, leading to the penetration of Ag^+ ions from the melt into the substrate, where they replace the Na^+ ions balancing the concentration gradient in the opposite direction. The intensity of the diffusion or concentration gradient decreases with the depth of the substrate, forming a diffusion profile that is a function of spatial coordinates. In this case, we can speak of diffusion from an infinite source of impurities. The parameters of the waveguide formation process can be controlled by the melt temperature, the concentration of ions in the melt, and the duration of the process. The channel waveguide is thus formed in contact with the surrounding environment at the substrate surface. Thus, in this region, a strong evanescent wave is generated, which can be advantageously used in contrast to the use of full two-step ion exchange used in our previous works in Barkman et al. (2013) and Smejcky et al. (2021).

In the next step, the PMMA layer doped with Porphyrine dye was deposited by spin coating (Fig. 4d). A Porphyrine solution dissolved in 1,2-dichloroethane was mixed with PMMA dissolved in the same way to a final solution by volume at a concentration such that the resulting mass concentration of porphyrin in PMMA was 3.5 wt%. The amount of dye was optimized experimentally. The low value resulted in a small modulation depth modulation (amplitude) of the grating, while a high value led to polymer degradation and disturbance of the periodicity of the optical grating. The merged solutions were stirred for 60 min in an ultrasonic bath. After the deposition, the substrate with waveguides is cut and facets polished (Fig. 4e).

The subsequent fabrication process of the BG patterning technique LBW was based on the Marangoni effect (Malkin 2008). The heat caused by the absorbed laser radiation heats the polymer over the transition temperature and begins to melt. The temperature gradient, as well as the surface tension gradient in the opposite direction, is generated by the scanning of the laser beam. The future grating surface line is then formed by the resulting so-called Marangoni phenomenon, which is causing the melted polymer mass to be re-distributed to the regions with higher surface tension thus at a lower temperature. Finally, if the sample is continuously mechanically moved in parallel to the scanner, it produces gratings. The polymer was doped with absorbent dye to increase absorption in the wavelength of the laser source used, increasing the inductive heat required for melting. The structure of the grating (grating period and modulation depth) is then directly determined by the polymer dopant concentration, laser beam intensity, and sample speed. Olympus Lext OLS 3100 confocal laser scanning microscope operating at a wavelength of 405 nm with laser power of 100 μW was used. The sensor fabrication procedure is depicted in Fig. 4.

3 Hybrid PWBG sensor characterization

Spectral characterization of temperature and relative humidity was performed in the climatic chamber and the shift of the Bragg attenuation dip depending on the change in environmental parameters was evaluated. Tests of the influence of the environment and its changes were carried out in the climatic test chamber VTSCH VC37018. This climate chamber with a closed temperature and relative humidity control system allowed a temperature change in the range of − 75 °C to 180 °C and relative humidity in the range of 10–98%. The temperature and relative humidity of the air had been set with high precision, while the high velocity of the circulating air ensured an even distribution of temperature and humidity in the test space. The required environmental conditions were preprogrammed for different types of stress tests. The measurement and the control of the surface temperature were two-fold, first, the internal sensor of the climate chamber located below the sample, and second the calibrated IR camera Fluke Ti25 for measuring the sample mass itself.

The fabricated samples were measured with the use of the set-up for the measurement of the optical spectral transmission power. The HL-2000 halogen lamp was used as the broadband source emitting in the wavelength range of 360–2400 nm. The sample was connected through SM optical fibers to the HP 86140A halogen source and the optical spectral analyzer HP 86140A. The insertion losses of PWBG were $IL = 1.2$ dB at a wavelength of 1310 nm. The sensor was measured in the temperature range of − 10 °C to 70 °C, at a set constant relative humidity of 50% RH, to avoid the effect of changes caused by increased absorption of water molecules into the sensor layer. The transmission spectral measurement setup and a control image from the integrated IR camera showing the heated sample are shown in Fig. 5.

The spectral dip of fabricated PWBG at room temperature si shown in Fig. 6a. Figure 6b, c shows the measured temperature dependence of the Bragg attenuation dip wavelength position λ_B. The change in the spectral position of the Bragg attenuation dip for selected temperatures is shown in Fig. 6b. Figure 6c depicts the evaluation of the measured and theoretical change in the position of the Bragg wavelength attenuation dip of the fabricated PWBG sensor. The λ_B position shifts to the region of lower wavelengths with an accompanying slight decrease in the magnitude of the attenuation in the dip over the temperature range T_t of − 10 °C to 70 °C with increasing temperature.

The cause of the attenuation change is a decrease in the refractive index of the PMMA layer due to temperature (negative thermo-optic coefficient for PMMA polymer) resulting

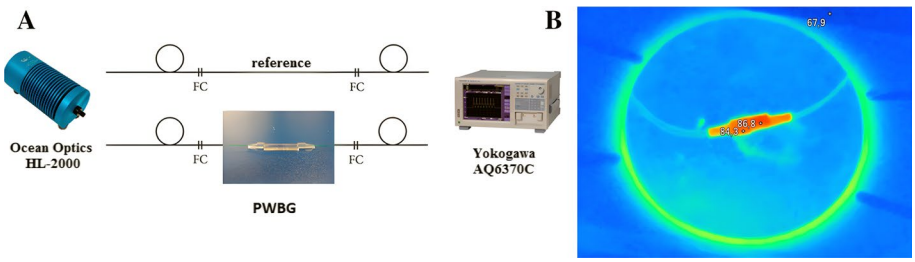

Fig. 5 **a** The transmission spectral measurement setup; **b** the image of the PWBG sensor under testing inside the chamber using an IR camera (the heated sample is shown in red). (Color figure online)

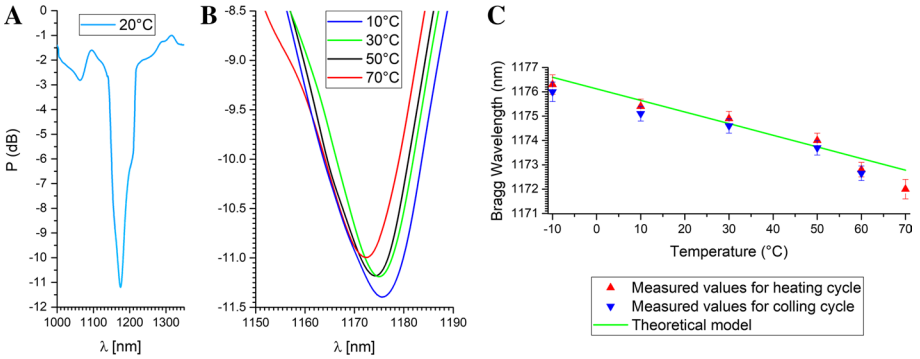

Fig. 6 **a** The spectral dip of PWBG at room temperature; **b** the detail of spectral change of dependence Bragg attenuation dip on temperature; **c** measured and theoretical approximated Bragg wavelength attenuation dip dependence on temperature produced by hybrid PWBG sensor

in a decrease of the evanescent field intensity causing reduced evanescent wave interaction with the grating and resulting in reduced diffraction efficiency. The change in the refractive index n_{PMMA} of the PMMA layer n_{eff} and the spectral shift λ_B to lower wavelengths confirm the theoretical assumption caused by the higher negative thermo-optical coefficient PMMA $dn_{eff}/dT = -130 \cdot 10^{-6}$ °C^{-1} compared to the positive coefficient of longitudinal expansion PMMA $\alpha' = 50 \cdot 10^{-6}$ °C^{-1}. The theoretical model of the Bragg wavelength on the temperature, which was calculated based on the relation (6) and the measured values of the displacement of minima λ_B are shown in Fig. 7b. The results show a good agreement between the theoretical and measured temperature sensitivity with a value of −56.6 pm °C^{-1}. In terms of hysteresis of temperature sensing, after the heating to 70 °C, the sensor exhibited low hysteresis in the cooling cycle, however, the hysteresis value was withín to the measurement uncertainty.

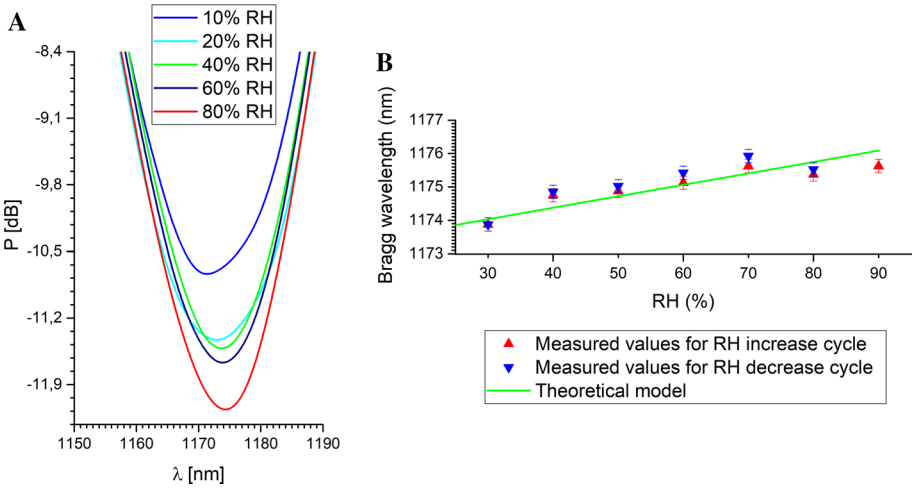

Fig. 7 **a** The spectral change of the Bragg attenuation dip position as a function of RH; **b** Measured and theoretical change of the Bragg attenuation dip position of the fabricated hybrid PWBG sensor as a function of RH

The characterization of the relative humidity detection was performed in the range of RH = 10–90%, at the selected constant temperature $T_t = 30$ °C. The temperature was chosen to ensure sufficient saturation of the water vapor in the air enclosed in the climate chamber for the selected RH measurement range while avoiding the influence of temperature T_t on changes in λ_B. The measured change in the spectral position of the λ_B attenuation dip due to humidity is shown in Fig. 7.

The dependence of the spectral position of λ_B on humidity is evident, whereby with increasing RH there is a shift of λ_B to the higher wavelength region, which is accompanied by an increase in the magnitude of the attenuation dip (up to 1.5 dB) over the RH = 10–90% relative humidity range. The absorption of water molecules into the cladding layer results in a higher refractive index which strengthens the evanescent field interacting with the grating. Hence, this results in a higher coupling coefficient and diffraction efficiency.

Unlike the increase in temperature, where the higher negative thermo-optic coefficient resulted in a λ_B shift to the shorter wavelengths, in the case of an increase in humidity, both coefficients are positive with values of the change in the refractive index change $dn_{eff}/dRH = 8.053 \cdot 10^{-6}$ and the length elongation due to moisture $\zeta = \Delta\Lambda/\Lambda = 2.123 \cdot 10^{-5}$. This results in a measured shift of λ_B to the higher wavelengths, see Fig. 7b. From the measured humidity dependence, it can be concluded that the measured λ_B shift agrees with the theoretical calculation of the proposed model according to the relation (8) in the range of RH = 10–70%. For RH = 70%, the maximum saturation of the PMMA layer with water molecules occurred, and a further increase in RH did not lead to a further wavelength shift. The resulting sensitivity of the hybrid PWBG to changes in humidity in the RH = 10–70% range is 54.16 pm/RH. In the case of relative humidity sense hysteresis, negligible hysteresis was present for the RH levels above 60%.

4 Conclusions

Properties of the hybrid planar optical PWBG sensor have been presented. The sensor was realized using two technology steps including fabrication of optical channel waveguides by ion exchange in the glass substrate and fabrication of polymer layer with Bragg grating onto this channel. Where the BGs were fabricated by the DLW method of the laser-thermal patterning technique based on the Marangoni effect.

Based on the experimental and theoretical results, the topological parameters of the PWBG sensor were optimized by BMP and RCWA algorithms to obtain a maximum diffraction efficiency of 97%. Third-order polymer PWBGs with the grating constant $\Lambda_{q\text{-}3} = 1.2$ μm were fabricated. The fabricated hybrid PWBGs sensor exhibits third-order diffraction documented by measurement of the optical spectral transmission characteristics. A significant dip at $\lambda = 1175$ nm at room temperature was observed, which correlated with the calculation. The attenuation of the spectral transmission was greater than 11 dB in the dip. Thus, a higher than 95% diffraction efficiency was achieved.

The measured sensitivity of PWBG was − 48.6 pm/°C, which is close to the theoretically calculated value of − 56.6 pm/°C. The resulting measured sensitivity in the RH = 10–70% range was 54.16 pm RH^{-1}. The main goal of this work that was achieved successfully was the design and verification of a new type of temperature and humidity sensor with the new layout hybrid glass/PMMA composition. It was confirmed that the efficient handling and certain fabrication steps, such as cutting, polishing, and coupling, were easily accomplished, compared to the PWBG sensors based purely on the polymer materials. The

resulting coupling losses fiber–facet was only 0.2 dB. The total average insertion loss of the 1.2 dB PWBG sensor was determined.

Acknowledgements This work was supported in part by the Student Grant Competition of the Czech Technical University in Prague under the grant number of SGS20/175/OHK3/3T/13 and by the Centre of Advanced Applied Natural Sciences, Reg. No. CZ.02.1.01/0.0/0.0/16 _019/0000778, supported by the Operational Program Research, Development and Education, co-financed by the European Structural and Investment Funds and the state budget of the Czech Republic. The authors acknowledge fruitful cooperation in the fabrication process with experts from the Department of Solid State Engineering, University of Chemistry and Technology, Prague, Czech Republic, and SQS Vlaknova optika company.

Funding This work was supported in part by Centre of Advanced Applied Natural Sciences, Reg. No. CZ.02.1.01/0.0/0.0/16_019/0000778, supported by the Operational Program Research, Development and Education, co-financed by the European Structural and Investment Funds and the state budget of the Czech Republic.

Availability of data and material Not applicable.

Code availability Not applicable.

Declarations

Conflict of interest The authors declare that they have no conflict of interest.

References

Aubry, C., Trigaud, T., Moliton, J.P., Chiron, D.: Polymer gratings achieved by focused ion beam. Synt. Met. **127**(1–3), 307–311 (2002). https://doi.org/10.1016/S0379-6779(01)00644-0

Barkman, O., Jerabek, V., Prajzler, V.: Optical splitters based on self-imaging effect in multi-mode waveguide made by ion exchange in glass. Radioiengineering **22**(1) (2013)

Beneitez, N.T., Missinne, J., Shi, Y., et al.: Highly sensitive waveguide Bragg grating temperature sensor using hybrid polymers. IEEE Photonics Technol. Lett. **28**(10), 1150–1153 (2005). https://doi.org/10.1109/LPT.2016.2533020

Binfeng, Y., Guohua, H., Yiping, C.: Polymer waveguide Bragg grating Fabry–Perot filter nanoiprinting technique. IOP J. Photonics **16**, 105501 (2014). https://doi.org/10.1088/2040-8978/16/10/105501

Carroll, K.E., Zhang, C., David, J., Webb, D.J., et al.: Thermal response of Bragg gratings in PMMA microstructured optical fibers. Opt. Express **15**(14), 8844–8850 (2007). https://doi.org/10.1364/OE.15.008844

Dobb, H., Webb, D.J., Kalli, K., et al.: Continuous wave ultraviolet light-induced fiber Bragg gratings in few- and single-mode microstructured polymer optical fibers. Opt. Lett. **30**(24), 3296–3298 (2005). https://doi.org/10.1364/OL.30.003296

Johnson, D.I., Town, G.E.: Refractive index and thermo-optic coefficient of composite polymers at 1.55 μm. In: SPIE Proceedings of the Conference on Microelectronics—Design, Technology and Packaging II, Brisbane (Australia), vol. 6038, no. 603821 (2015). https://doi.org/10.1117/12.656497

Liu, H.Y., Peng, G.D., Chu, P.L.: Thermal tuning of polymer optical fiber bragg gratings. IEEE Photon. Technol. Lett. **13**(8), 824–826 (2001). https://doi.org/10.1109/68.935816

Lyutakov, O., Huttel, I., Siegel, J., Svorcik, V.: Regular surface grating on doped polymer induced by laser scanning. Appl. Phys. Lett. Doi (2009). https://doi.org/10.1063/1.3254210

Malkin, A.Y.: Surface instabilities. Colloid J. **70**, 673–689 (2008). https://doi.org/10.1134/S1061933X0806001X

Mares, D., Jerabek, V.: Polymer waveguide Bragg gratings made by laser patterning technique. Opt. Quantum Electron. (2016). https://doi.org/10.1007/s11082-016-0438-9

Mizunami, T., Djambova, T.V., Niiho, T., Gupta, S.: Bragg gratings in multimode and few-mode optical fibers. J. Lightwave Technol. **18**(2), 230–235 (2000). https://doi.org/10.1109/50.822797

Ouerghia, F., Belhadja, W., Abdelmalek, F.: Polymer thin films and Bragg grating structures based temperature and pressure integrated effects. Thin Solid Films **485**(1–2), 176–181 (2005). https://doi.org/10.1016/j.tsf.2005.02.022

Reznikova, E., Mohr, J., Boerner, M., Nazmov, V., Jakobs, P.J.: Soft X-ray lithography of high aspect ratio SU8 submicron structures. Microsys. Technol. **14**(9–11), 1683–1688 (2008). https://doi.org/10.1007/s00542-007-0507-x

Rosenberg, M., Koller, G., Belle, S., Schmauss, B., Hellmann, R.: Planar Bragg grating in bulk Polymethylmethacrylate. Opt. Express **20**(25), 27288–27296 (2012). https://doi.org/10.1364/OE.20.027288

Rosenberg, M., Hessler, S., Belle, S., Schmauss, B., Hellmann, R.: Compressive and tensile strain sensing using a polymer planar Bragg grating. Opt. Express **22**(5), 5483–5490 (2014). https://doi.org/10.1364/OE.22.005483

Rosenberger, M., Hessler, S., Belle, S., Schmauss, B., Hellmann, R.: Humidity-Induced effects on polymer planar bragg gratings. IEEE Photonics Technol. Lett. **26**(16), 1669–1671 (2014). https://doi.org/10.1109/LPT.2014.2330656

Sherman, S., Zappe, H.: Printable Bragg gratings for polymer-based temperature sensor. In: Proceedings of the 2nd International Conference on System-Integrated Intelligence (SysInt)—Challenges for Product and Production Engineering. The Bremen (Germany), vol. 15, pp. 702–709 (2014). https://doi.org/10.1016/j.protcy.2014.09.041

Smejcky, J., Mares, D., Barkman, O., et al.: Er3+/Yb3+ doped active optic Y splitter realized by diffusion waveguides with Ag+–Na+ ion exchange. Opt. Quantum Electron. (2021). https://doi.org/10.1007/s11082-021-03035-2

Weber, M.: CRC Handbook of Laser Science and Technology Supplement 2: Optical Materials. CRC Press, Boca Raton (1995). ISBN 9780849335075

Wong, W.H., Pun, E.Y.B., Chan, K.S.: Electron beam direct-write tunable polymeric waveguide grating filter. IEEE Photonics Technol. Lett. **15**(12), 1731–1733 (2003). https://doi.org/10.1109/LPT.2003.819709

Yu, J.M., Tao, X.M., Tam, H.Y.: Trans-4-stilbenemethanol-doped photosensitive polymer fibers and gratings. Opt. Lett. **29**(2), 156–158 (2004). https://doi.org/10.1364/OL.29.000156

Zhang, Z.F., Tao, X.M.: Intrinsic temperature sensitivity of fiber Bragg gratings in PMMA-based optical fibers. IEEE Photonics Technol. Lett. **25**(3), 310–312 (2013). https://doi.org/10.1109/LPT.2012.2235421